Cerebral Cortex, July 2018;28: 2391–2404

doi: 10.1093/cercor/bhx141
Advance Access Publication Date: 7 June 2017
Original Article

ORIGINAL ARTICLE

Cholinergic Grb2-Associated-Binding Protein 1 Regulates Cognitive Function

Nan-Nan Lu[1], Chao Tan[1], Ning-He Sun[1], Ling-Xiao Shao[1], Xiu-Xiu Liu[1,2], Yin-Ping Gao[1,2], Rong-Rong Tao[1], Quan Jiang[1], Cheng-Kun Wang[1], Ji-Yun Huang[1], Kui Zhao[3], Guang-Fa Wang[3], Zhi-Rong Liu[4], Kohji Fukunaga[5], Ying-Mei Lu[2,6] and Feng Han[1]

[1]College of Pharmaceutical Sciences, Institute of Pharmacology and Toxicology, Zhejiang University, Hangzhou, Zhejiang 310058, China, [2]School of Medicine, Zhejiang University City College, Hangzhou, Zhejiang 310015, China, [3]Department of PET Center, The First Affiliated Hospital, Zhejiang University School of Medicine, Hangzhou, Zhejiang 310006, China, [4]Department of Neurology, Second Affiliated Hospital of Zhejiang University, School of Medicine, Hangzhou, Zhejiang 310009, China, [5]Department of Pharmacology, Graduate School of Pharmaceutical Sciences, Tohoku University, Aoba-ku, Sendai 980–8578, Japan and [6]Key Laboratory of Medical Neurobiology of Ministry of Health of China, Department of Neurobiology, Zhejiang University School of Medicine, Hangzhou, Zhejiang 310058, China

Address correspondence to Dr Feng Han, College of Pharmaceutical Sciences, Institute of Pharmacology and Toxicology, Zhejiang University, 866 Yu-Hang-Tang Road, Hangzhou, Zhejiang 310058, China. E-mail: changhuahan@zju.edu.cn; Dr Ying-Mei Lu, School of Medicine, Zhejiang University City College, Hangzhou, Zhejiang 310015, China. E-mail: lufx@zju.edu.cn

Nan-Nan Lu and Chao Tan contributed equally to this work

Abstract

Grb2-associated-binding protein 1 (Gab1) is a docking/scaffolding molecule known to play an important role in cell growth and survival. Here, we report that Gab1 is decreased in cholinergic neurons in Alzheimer's disease (AD) patients and in a mouse model of AD. In mice, selective ablation of Gab1 in cholinergic neurons in the medial septum impaired learning and memory and hippocampal long-term potentiation. Gab1 ablation also inhibited SK channels, leading to an increase in firing in septal cholinergic neurons. Gab1 overexpression, on the other hand, improved cognitive function and restored hippocampal CaMKII autorphosphorylation in AD mice. These results suggest that Gab1 plays an important role in the pathophysiology of AD and may represent a novel therapeutic target for diseases involving cholinergic dysfunction.

Key words: cholinergic neurons, cognitive dysfunction, Gab1, hyperexcitability, septo-hippocampal system

Introduction

Dysfunction of the central cholinergic systems has been suggested to play an important role in the pathogenesis of cognitive impairment (Ji et al. 2001; Goekoop et al. 2006; Gu and Yakel 2011; Pa et al. 2013). A causal relationship has been postulated between cholinergic dysfunction and the progression of cognitive decline in neurodegenerative disorders such as Alzheimer's disease (AD) (Christensen et al. 1992; Goekoop et al. 2006; Okada et al. 2013; Yang et al. 2013); however, the cause of the dysfunction remains unclear.

The Grb2-associated-binding protein 1 (Gab1) is a scaffold protein critically involved in signaling transduction (Schaeper et al. 2007; Eulenfeld and Schaper 2009). Tyrosine-phosphorylated Gab1 binds to a number of downstream signaling proteins, including GRB2, the p85 subunit of PI3K, and SHP-2 (Bard-Chapeau et al. 2005; Dixit et al. 2005; Mood et al. 2006; Lu et al. 2011). The Gab1/EGF receptor tyrosine kinase has been intensely studied in the peripheral nervous system, where it plays principal roles in the survival and target selectivity of sensory and sympathetic neurons (Bard-Chapeau et al. 2005; Schaeper et al. 2007; Yang et al. 2012). Gab1 has also been reported to mediate the differentiation, DNA synthesis, and cell survival of PC12 cells (Korhonen et al. 1999). More recently, cognitive dysfunction in the Angelman syndrome mouse has been correlated with a reduction of Gab1 in the brain (Cao et al. 2013).

The septo-hippocampal cholinergic system plays a crucial role in memory (Hangya et al. 2009; Kaifosh et al. 2013; Mitsushima et al. 2013). Impaired cholinergic innervation leads to reduced NMDA receptor function and impaired CaMKII activity in the hippocampus (Han, Shioda, Moriguchi, Yamamoto et al. 2008). Protein tyrosine phosphatase inhibitors, by stimulating tyrosine kinase receptor signaling and activating survival signals in the cholinergic medial septal neurons, improve hippocampal long-term potentiation (LTP) and memory-related behaviors (Han, Shioda, Moriguchi, Qin et al. 2008). Hence, protection of septal cholinergic neurons against degeneration may prevent or delay cognitive impairments in AD.

Here, we report that Gab1 is expressed in central cholinergic neurons and is decreased in human AD brain. Selective ablation of Gab1 in cholinergic neurons impairs hippocampal LTP and causes memory deficits in mice. In vivo rescue of Gab1 in the medial septum restores the cognitive function of *ChAT-Cre;Gab1$^{f/f}$* and *APP^{swe}/PS1* mice. These results suggest that Gab1 is essential for normal functioning of central cholinergic neurons and may serve as a novel target for the treatment of AD.

Materials and Methods

Transgenic Mice

Floxed Gab1 transgenic mice (*Gab1$^{f/f}$* or *Gab1$^{loxP/loxP}$*) (C57BL/6 background; kindly provided by Yue-hai Ke's lab at Zhejiang University) (Bard-Chapeau et al. 2005; Zhang et al. 2016) were bred with *ChAT-Cre* (Stock No. 006410, The Jackson Laboratory), *ChAT^{BAC}-eGFP* (Stock No. 007902, The Jackson Laboratory), and *CaMKIIα-Cre* mice (Stock No. 005359, The Jackson Laboratory) to generate *ChAT-Cre;Gab1$^{f/f}$*, *ChAT-eGFP;Gab1$^{f/f}$*, and *CaMKIIα-Cre;Gab1$^{f/f}$* mice. To assist electrophysiological recording of cholinergic neuron, the *ChAT-Cre;Gab1$^{f/f}$* mice were further crossed with *ChAT-eGFP;Gab1$^{f/f}$* mice to specifically label cholinergic neurons with enhanced green fluorescent protein (eGFP). *APP^{swe}/PS1* (B6.Cg-Tg (*APP^{swe}*,PSEN1dE9)85Dbo/Mmjax, Stock No. 34832) mice were obtained from the Jackson Laboratory. Genomic DNA extracted from mouse tails was amplified by PCR for genotyping. All mice were housed under a 12-h light/dark schedule and had access to food and water ad libitum. All experiments and protocols were approved by the Zhejiang University Animal Experimentation Committee and were in complete compliance with the National Institutes of Health Guide for the Care and Use of Laboratory Animals. Mice were allocated into different groups randomly. In the behavioral experiments, only male mice were used and behavioral experiments were performed double-blindly.

Adeno-Associated Virus or Lentiviral Vector Preparation and Stereotaxic Brain Delivery

To focally reduce endogenous Gab1 levels in the medial septum, adeno-associated virus (AAV)2-Cre-GFP was stereotaxic injected into medial septum of *Gab1$^{f/f}$* mice (8 weeks old). Based on AAV serotype 2, AAV2-Cre-GFP expresses Cre recombinase and GFP under the human cytomegalovirus (CMV) immediate early promoter. AAV2-Cre-GFP virus (6.9×10^{12} GC/mL) was packaged by Sunbio medical biotechnology.

To selectively express Gab1 in the cholinergic neuron in medial septum in *ChAT-Cre;Gab1$^{f/f}$* mice (8 weeks old), the AAV-Flex-Gab1 and AAV-Flex-Con vectors were designed and constructed by standard methods. Full length cDNA of Gab1 with a Myc tag in C-terminal was inserted into the AAV-Flex backbone (cloned from AAV-FLEX-rev-ChR2-tdtomato, Addgene plasmid #18917) with *Kpn*I and *Bam*HI to generate AAV-Flex-Gab1. EGFP were inserted into the same backbone with the same restriction sites to generate AAV-Flex-Con vector. AAV-Flex-Gab1 virus (1.9×10^{12} GC/mL) and AAV-Flex-Con virus (1.1×10^{12} GC/mL) of AAV2/9 serotype were packaged by Hanbio Biotechnology.

To overexpress Gab1 in the medial septum in *APP^{swe}/PS1* AD model mice (6 months old), a lentiviral vector expressing Gab1 (lentiviral-Gab1 or lenti-Gab1) and control virus (lentiviral-Con or lenti-Con) were used. To construct a lentiviral vector expressing Gab1, two complementary Gab1 DNA oligonucleotides were synthesized and inserted into the *Eco*RI–*Bam*HI site of the transfer vector pCDH-CMV-MCS-EF1-copGFP under the control of the CMV promoter. The constructed vector was then transformed into *Escherichia coli* $DH_{5\alpha}$ and extracted. A large-scale production of lentiviral-Gab1 was performed via transfection of HEK293T cells (Tao et al. 2014). Lentiviral-Gab1 (1.10×10^8 TU/mL) and lentiviral-Con (3.10×10^9 TU/mL) were used.

For the delivery of AAV or lentiviral, mice were anesthetized with 2% isoflurane and mounted on a custom-built mouse stereotaxic device during surgery. Eye drops were used to avoid drying. The animals received stereotaxic injections of virus (1 μL) into the medial septum at the coordinates AP + 0.8 mm, ML 0 mm, DV −3.8 mm. To minimize tissue injury, the virus was delivered with a glass microelectrode with a 10- to 20-μm diameter tip into the target coordinates over a 10 min period with a WPI Nanoliter 2000 Injector. Three weeks after the introduction of the viral vectors, the behavioral tests were performed.

Electrophysiology

We made slices containing the medial septum from 2 to 3 weeks old postnatal mice or adult mice injected with AAV virus. For 2 to 3 weeks old postnatal mice, the slices (300 μm) were prepared with a Vibroslice (Leica VT 1000S, USA) in ice-cold cutting artificial cerebrospinal fluid (ACSF) consisting of (in mM) 125 NaCl, 3 KCl, 1.25 NaH_2PO_4, 2 $MgSO_4$, 2 $CaCl_2$, 25 $NaHCO_3$, and 10 glucose saturated with 95% O_2 and 5% CO_2. The slices were allowed to recover for 30 min at 34°C in the same oxygenated ACSF and then kept at room temperature (22°C) before being transferred to the recording chamber. For adult mice injected with AAV virus, the cutting ACSF was replaced by another solution as follows (in mM): 75 sucrose, 87 NaCl, 2.5 KCl, 1.25 NaH_2PO_4, 7 $MgCl_2$, 0.5 $CaCl_2$, 26 $NaHCO_3$, and 25 glucose.

Fluorescence images of neurons were visualized under an upright microscope with a 40× water-immersion lens (Olympus) and the whole-cell patch clamp recordings were carried out (MultiClamp 700B Amplifier, Digidata 1440A analog-to-digital

converter). Data were acquired and analyzed with pClamp 10.2 software (Axon Instruments/Molecular Devices) as previously described (Li et al. 2011). To record action potentials (APs) in cholinergic neurons, glass micropipettes (3–4 MΩ) were filled with a solution containing (in mM) 130 potassium gluconate, 20 KCl, 10 HEPES, 4 Mg-ATP, 0.3 Na-GTP, 10 disodium phosphocreatine, and 0.2 EGTA (pH 7.25 was adjusted with KOH and osmolarity was 288 mOsm). For *ChAT-Cre;Gab1$^{f/f}$* mice injected with AAV-Gab1, putative cholinergic neurons were recorded and identified by intracellular injections of Lucifer yellow and post hoc staining. To investigate whether SK channels were involved in abnormal APs, its agonist (NS309, 5 μM, Tocris Bioscience) or antagonist (apamin, 100 nM, Tocris Bioscience) was applied in the ACSF.

For analysis of the passive membrane properties of cholinergic neurons, data analyses were performed after obtaining the whole-cell configuration. Input resistance (R_{in}) was calculated from small voltage deflections induced by rectangular hyperpolarizing current injections (0–60 pA, 10 pA steps). Membrane time constant (τ_m) was obtained by fitting a single exponential function to hyperpolarizing voltage deflection (40 pA). Membrane capacitance (C_m) was derived by dividing τ_m by R_{in}.

For LTP recordings, hippocampal slices were prepared from adult *ChAT-Cre;Gab1$^{f/f}$* and *Gab1$^{f/f}$* mice as previously described (Gong et al. 2009). Transverse slices (400 μm thick) were prepared with a vibroslice in ice-cold ACSF, then incubated for 2 h in continuously oxygenated ACSF (95% O_2, 5% CO_2) at room temperature. The slices were transferred to a recording chamber and superfused with warm ACSF (34°C) at a flow rate of 2–3 mL/min. The stimulating electrode was placed at the Schaffer collateral/commissural pathway and evoked field excitatory postsynaptic potential (fEPSP) was recorded from the stratum radiatum of CA1 using a glass electrode filled with 3 M NaCl. LTP was induced by strong high-frequency stimulation (HFS, twice 100 Hz, 1 s trains, 20 s apart). Recording was performed using a single-electrode amplifier. Data acquisition and analysis were performed in pClamp 10.2 software.

Behavioral Analyses

The novel object recognition test (NORT) was used to evaluate recognition memory (Han, Shioda, Moriguchi, Yamamoto et al. 2008). Briefly, mice were individually habituated to an open field box (35 × 25 × 35 cm) for 2 consecutive days. The experimenter who scored the behavior was blind to the treatment. Discrimination index was evaluated by comparing the difference between the time of exploration of the novel and familiar object and the total time spent exploring both objects, which made it possible to adjust for differences in total exploration time.

The assessment of spatial memory in the mice was carried out using the Y-maze task (Han, Shioda, Moriguchi, Yamamoto et al. 2008). The apparatus consisted of 3 identical black Plexiglas arms ($l \times w \times h$, 50 × 16 × 32 cm). The sequence of arm entries was recorded visually during an 8-min session, and 3 consecutive choices were defined as an alternation. Spontaneous alternation behavior in the Y-maze task was recorded, and the percentage of alternation was calculated as (actual alternations/maximum alternations) × 100.

The assessment of spatial learning and memory in mice were carried out using the Morris water maze (MWM) (Morris 1984). The movements of the mice were recorded using a video-tracking system. All mice were trained to find a hidden platform placed in the middle of the target quadrant. A 60 s probe test was conducted at day 6 after 5-day training, in which the platform was removed from the pool. The data were processed and analyzed for each acquisition trial or probe trial as the escape latency (in seconds), the times of platform crossing (in numbers) and time in target quadrant (in seconds).

A grip strength meter (Bio-Will Co., Ltd) was used to assess neuromuscular function as the maximal muscle strength of forelimbs of mice. Maximal muscle strength was measured by the grasping force applied by the mouse on a grid that was connected to a sensor. Three trials were carried out in succession to measure forelimb strength per animal.

Immunohistochemistry

Mice were anesthetized and transcardially perfusion-fixed with 4% paraformaldehyde in phosphate-buffered saline (PBS). For immunohistochemistry, coronal sections (45-μm thick) were incubated at room temperature with blocking buffer (0.1% Triton X-100 and 3% BSA in PBS) (Han, Shioda, Moriguchi, Yamamoto et al. 2008). Fixed and permeabilized sections were incubated with anti-Gab1 (1:200, Cell Signaling Technology), anti-ChAT (1:500, Millipore), anti-GAD65 (1:1000, Alpha Diagnostic International), anti-parvalbumin (1:200, Millipore), anti-CaMKIIα (1:300, Abcam), anti-β-amyloid 1-40/42 (1:200, Alpha Diagnostic International), anti-phospho-tau-Ser-404 (1:200) (Ishiguro et al. 1995), anti-VAchT (1:500, Abcam), anti-phospho-Thr286-CaMKII (1:300) (Fukunaga et al. 1988), and anti-MAP-2 (1:1000, Millipore) overnight at 4°C (Liu et al. 1999). Immunofluorescent images were visualized by confocal laser-scanning microscopy (Zeiss LSM 510). The 3D filled plots were processed by using ImageJ v1.45 (NIH) with the accompanied "Interactive 3D Surface Plot" plug-in.

The post hoc immunocytochemistry was used to identify the cholinergic neurons. After electrophysiological recording, brain slices include that lucifer yellow-filled neurons in MS were fixed with 4% paraformaldehyde overnight at 4 °C. The brain slices were incubated with a primary antibody against ChAT (1:500, Millipore) and lucifer yellow (1:1000, Invitrogen) in PBS containing 5% goat serum and 0.3% Triton X-100 for 24 h. Samples were then washed and incubated with secondary antibody (Alexa fluor 488-conjugated anti-rabbit IgG and Alexa fluor 594-conjugated anti-goat IgG, Invitrogen) for 6 h at room temperature. Labeled neurons were visualized with a confocal laser-scanning microscope (Nikon A1).

Quantification of percentages of Gab1-positive cells coexpressing ChAT ($ChAT^+/Gab1^+$) and percentages of ChAT-positive cells coexpressing Gab1($Gab1^+/ChAT^+$) were achieved by using the ImageJ Cell Counter analysis tool (NIH). Quantification of the density of Gab1-positive cells per mm^2 of brain area was achieved by counting the Gab1-positive cell number of randomly selected fields (634 × 634 μm). Totally, 9 randomly selected fields of each brain region (medial septum, striatum, and cortex) were analyzed from 3 nonadjacent sections per mouse.

Western Blot Analysis

Hippocampal CA1 samples and medial septum from mice were homogenized, and western blots were carried out according to protocols as previously described (Lu et al. 2014; Wang et al. 2015). Samples containing equivalent amounts of protein were subjected to sodium dodecyl sulfate–polyacrylamide gel electrophoresis and transferred to a polyvinylidene difluoride membrane (Millipore). After blocking with TTBS solution (20 mM Tris–HCl, pH 7.4, 150 mM NaCl, and 0.1% Tween 20) containing 5% skimmed milk for 1 h, the membranes were incubated overnight at 4°C and protein were detected by immunoblot using the following primary antibodies: anti-Gab1

and anti-Gab2 (1:1000, Cell Signaling Technology), phospho-Thr286-CaMKII (1:3000) (Fukunaga et al. 1988), CaMKII (1:3000) (Fukunaga et al. 1988), phospho-Synapsin I-Ser603 (1:2000, Millipore), Synapsin I (1:2000) (Fukunaga et al. 1992), and anti-β-actin (1:10 000, Sigma). Immunoreactive band intensities were analyzed by ImageJ software (NIH). The band was normalized against the corresponding β-actin band used as loading control.

Postmortem AD Brain Samples

Cortex sections of postmortem human brain samples were provided by China Brain Bank of Zhejiang University. All materials have been collected from donors who have written informed consent for brain autopsy. Cortex sections from one case of pathologically confirmed AD (91 years old) and one case of non-demented control (60 years old) were collected, fixed in formalin, and embedded in paraffin. Subsequently, 6 μm-thick sections were cut and processed for immunohistochemistry staining of Gab1 (Cell Signaling Technology) and ChAT (Millipore). The research was approved by the Medical Ethical Committee of Zhejiang University School of Medicine (No. 1-009).

MicroPET/CT Scan

Mice were anesthetized with 2% isoflurane in O_2 gas and intravenously injected with approximately 0.45 mCi of ^{18}F-FDG. MicroPET/CT scans were performed and images were reconstructed as previously reported (Mahmood et al. 2017). Briefly, mice were placed pronely in the center of Siemens Inveon combined microPET-CT scanner (Siemens Preclinical Solution USA, Inc.) under continuous anesthesia inhalation (2% isoflurane in O_2 gas). A 10 min PET static acquisition was performed and the images were reconstructed using OSEM (ordered set expectation maximization) algorithm for 3D PET reconstruction. The data in DICOM format were exported and analyzed with Matlab software. The standardized uptake value (SUV) was obtained with the formula SUV = RTA/RID × BW, where RTA is the measured radiotracer tissue activity (in mCi), RID is the radiotracer injected dose (in mCi), and BW is the mouse body weight (in g). The brain of each mouse was registrated to a reference atlas to measure radiotracer uptake (SUV) in different structures of brain (Johnson et al. 2010).

Statistical Analysis

Data are presented as mean ± standard error of the mean (SEM). Unless otherwise noted, statistical differences were determined by either unpaired two-tailed Student's *t*-test or one-way analysis of variance (ANOVA), followed by Tukey's post hoc test, with $P < 0.05$ considered to indicate a significant difference.

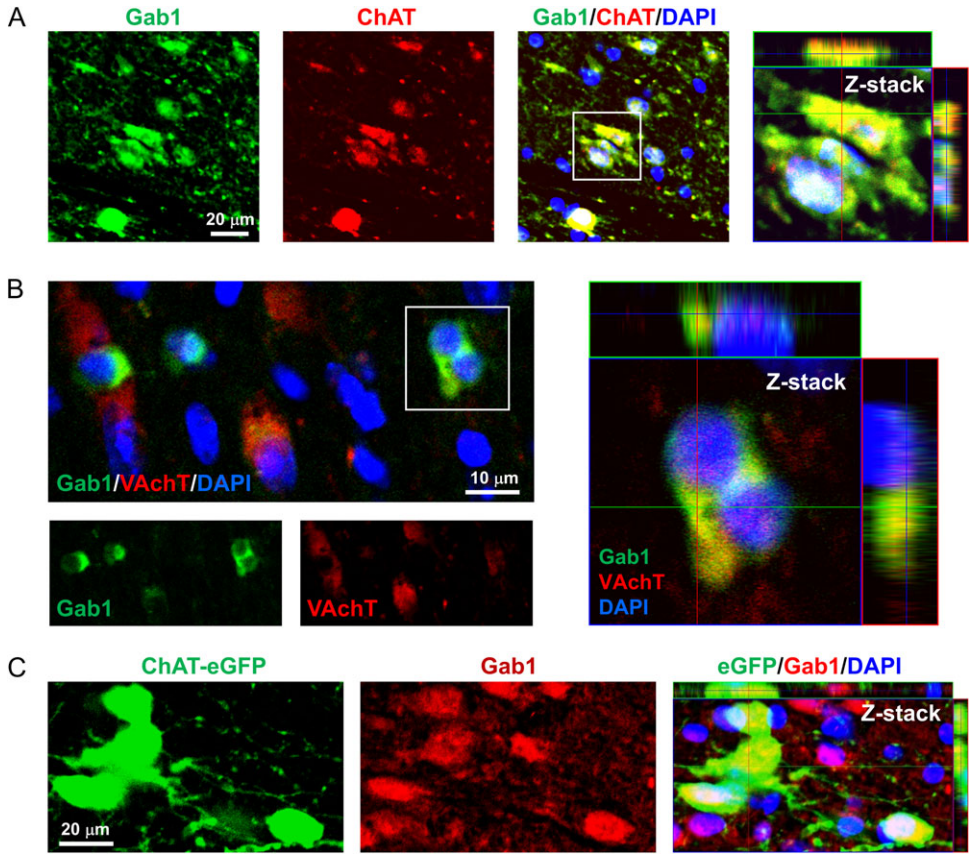

Figure 1. Cell type-specific distribution of Gab1 in the adult mice brain. The subcellular localization of Gab1 in the medial septum of adult mice was determined by laser confocal microscopy. (*A*) Immunohistochemistry for Gab1 (green), ChAT (red), and merged expression (orange-yellow) showed colocalization of Gab1 with ChAT in the medial septum (scale bar, 20 μm). Overlapping red and green pixels appear as orange-yellow, depicted in the Z-stack image. (*B*) Gab1 colocalized with VAchT-positive neurons in mice brain. The confocal image showed that Gab1 was colocalized with the cholinergic neuron marker VAchT in medial septum (scale bar, 10 μm). Overlapping red (VAchT) and green (Gab1) pixels were depicted as the Z-stack image. (*C*) Representative immunostaining data showing a majority of the Gab1 colocalized with the ChAT-eGFP-positive neurons in medial septum. DAPI counterstaining indicated nuclei (blue) (scale bar, 20 μm).

Results

Gab1 is Selectively Expressed in Central Cholinergic Neurons

Using immunostaining we found that Gab1 was expressed in the medial septum and showed colocalization with choline acetyltransferase (ChAT) (Fig. 1A). Gab1-positive cells also stained positively for the vesicular acetylcholine transporter (VAChT), another marker of cholinergic neurons (Fig. 1B). Consistent with these results, the majority of Gab1-positive cells expressed GFP in *ChAT*^{BAC}*-eGFP* mice (Fig. 1C). What's more, quantitative analysis data from whole brain suggested that a quite high proportion Gab1-positive cells are cholinergic neurons, 93.3 ± 3.1% in the medial septum, 91.2 ± 0.7% in the striatum, and 97.3 ± 0.7% in the cortex, respectively. The percentages of ChAT-positive cells coexpressing Gab1 are 83.4 ± 1.5% in the medial septum, 54.7 ± 7.7% in the striatum, and 92.9 ± 1.0% in the cortex (Supplementary Fig. 1A). The density of Gab1-expressing cells in the medial septum (159.0 ± 15.27 per mm^2) is higher than striatum (24.58 ± 8.32 per mm^2) and cortex (75.21 ± 22.30 per mm^2) (Supplementary Fig. 1B). In contrast, no colocalization of Gab1 was observed with GAD65 (Supplementary Fig. 2) and parvalbumin (Supplementary Fig. 3). Both are markers of GABA neurons. In addition, there was also no colocalization of Gab1 with CaMKIIα, a marker for excitatory neurons, which excludes the expression pattern of Gab1 in excitatory neurons (Supplementary Fig. 4).

Downregulation of Gab1 in AD Patient and *APP*^{swe}*/PS1* Mice

Neurons stained for Gab1 were found to colocolize with ChAT and neurons stained for both were found throughout the cerebral cortex in a 60-year-old normal control (Fig. 2A). A strong

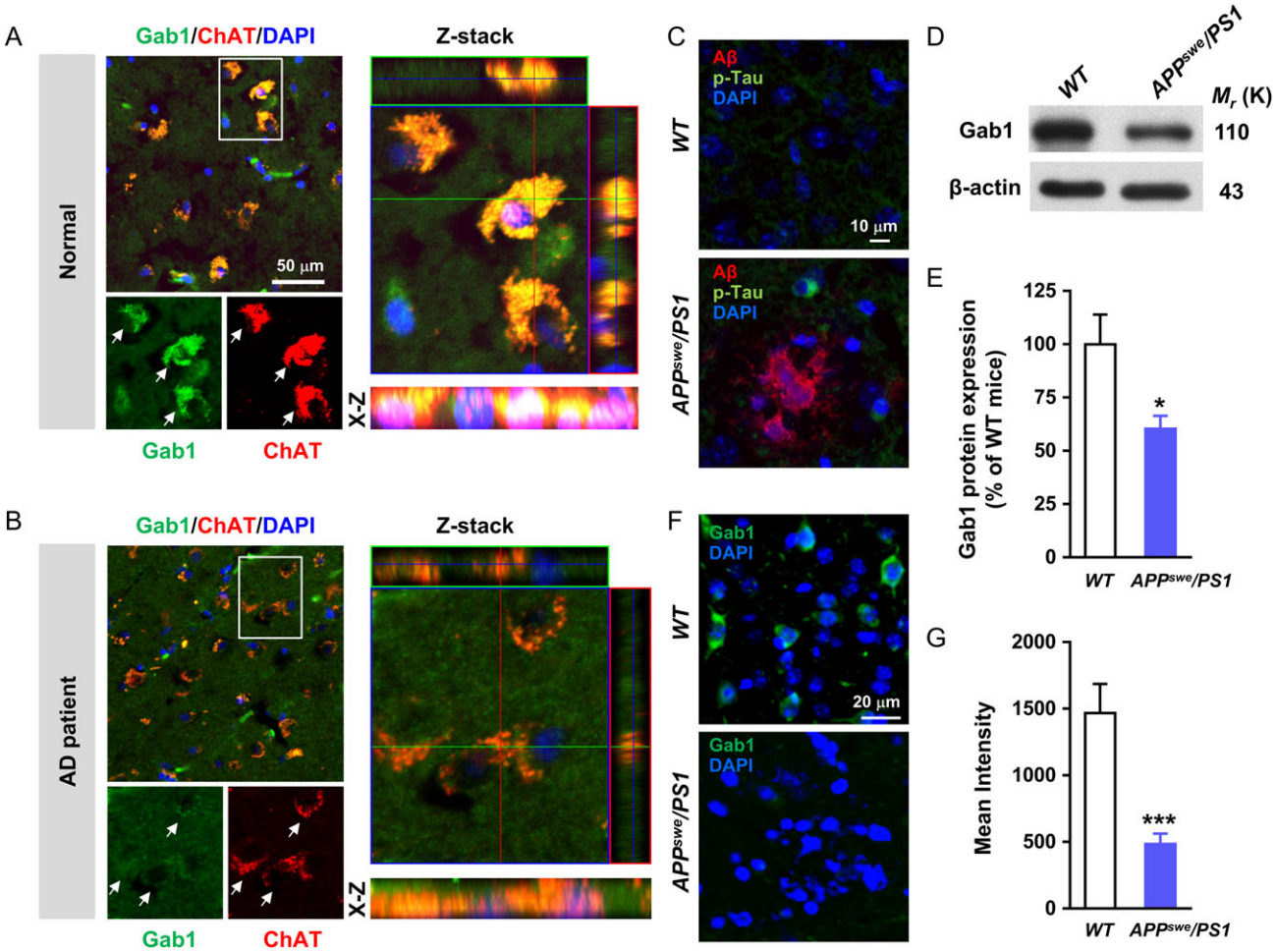

Figure 2. Decreased Gab1 protein levels in AD patient and *APP*^{swe}*/PS1* AD model mice. (*A*) Brain cortex sections of aged normal control immunostained with the Gab1 (green) and cholinergic neuron markers ChAT (red) (scale bar, 50 μm). Right, higher-magnification Z-stack image of cholinergic neurons from the insets of left. Arrow indicates Gab1 expression in cholinergic neuron. (*B*) Reduced Gab1 expression in ChAT-positive cholinergic neurons is visible in brain cortex of AD patient (Arrow). Representative Z-stack images from the insets of left shown in right. Arrow indicates loss of Gab1 expression in cholinergic neuron. (*C*) Immunohistochemical localization of phosphorylated Tau (p-Tau, green) and β-amyloid (Aβ, red) in 6 months old *APP*^{swe}*/PS1* mice, and age-matched wide type (WT) mice. Neuronal staining of phosphorylated Tau (Ser-404) (green) is predominantly localized around accumulated β-amyloid (red) in 6 months old *APP*^{swe}/PS1 mice (scale bar, 10 μm). (*D*) Representative western blots of Gab1 from the medial septum of *APP*^{swe}*/PS1* and WT mice. Immunoblotting with an anti-β-actin antibody demonstrated equal protein loading in each lane. (*E*) Densitometry of western blots for Gab1. Data are expressed as densitometry ratio of WT. $^{*}P < 0.05$ versus WT mice using unpaired two-tailed Student's *t*-test. $n = 6$ mice of each group. (*F*) Representative immunostaining data showing a significant decreasing of Gab1 (Green) in medial septum in *APP*^{swe}*/PS1* mice when compared with WT mice (scale bar, 20 μm). (*G*) Quantification of Gab1 immunofluorescence expressed as mean intensity. $^{***}P < 0.001$ versus WT mice using unpaired two-tailed Student's *t*-test. DAPI counterstaining indicated nuclei (blue). WT ($n = 5$) and *APP*^{swe}*/PS1* ($n = 7$). Error bars represent mean ± SEM.

reduction in Gab1 was found in same region in a 91-year-old AD patient (Fig. 2B). In $APP^{swe}/PS1$ mice, a mouse model of AD, similar results were obtained. At 6 months of age, a significant increase in β-amyloid accumulation and hyperphosphorylation of Tau (Ser-404) were observed (Fig. 2C). These changes were accompanied by a 40% decrease in Gab1 in the septum as shown by immunoblotting (Fig. 2D,E) and immunohistochemistry (Fig. 2F,G). Thus, Gab1 appears to be selectively expressed in cholinergic neurons and is downregulated in both an AD patient and an animal model of AD.

Selective Downregulation of Gab1 in the Medial Septum Causes Cognitive Deficits

Recombinant AAV2-GFP vectors coding for Cre recombinase (AAV2-GFP-Cre) or scrambled-sequence AAV2 for control were injected into the medial septum of 8 weeks old $Gab1^{f/f}$ mice (Bennett et al. 2000). Gab1 expression was markedly suppressed in Cre expressing neurons 3 weeks after the injection (Fig. 3A). The same injection had no effect on Gab2 expression (Fig. 3B). Silencing of Gab1 had no effect on grip strength (Supplementary Fig. 5A), but it caused a significant decrease in discrimination index in the NORT (Fig. 3C) and a reduced success rate in the Y-maze test (Fig. 3D).

Loss of Gab1 in Cholinergic Neurons Leads to Cognitive Dysfunction in Adult Mice

To inhibit Gab1 expression more selectively in cholinergic neurons, mice carrying a loxP-flanked Gab1 gene were crossed with *ChAT-Cre* mice to produce conditional Gab1 knockout mice ($ChAT\text{-}Cre;Gab1^{f/f}$) (Fig. 4A). These mice again showed no change in grip strength (Supplementary Fig. 5B) and Gab2 expression (Fig. 4B). Unlike $ChAT\text{-}Cre;Gab1^{f/f}$ mice in which Gab1 expression was completely suppressed (Fig. 4C), $CaMKII\alpha\text{-}Cre;Gab1^{f/f}$ mice exhibited a wild type-like Gab1 expression pattern. No significant changes were observed in the number and size of Gab1-positive neurons (Supplementary Fig. 6).

In the novel object recognition task, $ChAT\text{-}Cre;Gab1^{f/f}$ mice exhibited a reduced ability to discriminate familiar from novel objects (16.1 ± 5.3%, Fig. 4D) compared with $Gab1^{f/f}$ mice (44.9 ± 9.1%). In the Y-maze task, the $ChAT\text{-}Cre;Gab1^{f/f}$ mice (50.6 ± 7.3%) also exhibited a significant decrease in alternation behaviors compared with $Gab1^{f/f}$ mice (83.2 ± 2.9%) (Fig. 4E).

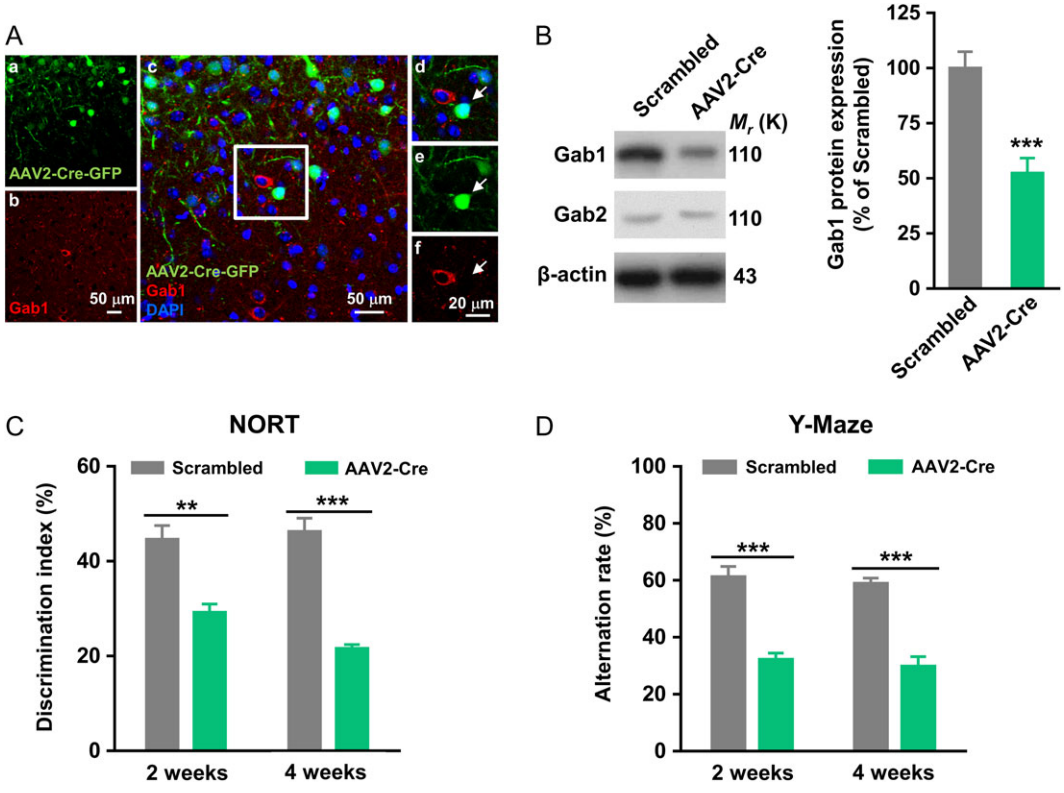

Figure 3. Loss of Gab1 in medial septum leads to cognitive dysfunction. (A) The distribution of AAV2-Cre-GFP in the medial septum of $Gab1^{f/f}$ mice 3 weeks after microinjection. The images demonstrate successful AAV2-Cre-GFP transduction in the brain. Images of brain slices from a $Gab1^{f/f}$ mouse 3 weeks after AAV virus injection show sparse Cre expression (green) in the medial septum (a). The low expression level of Gab1 (red) in Cre expression neurons indicates that our strategy successfully leads to the loss of Gab1 in medial septum, as showed in higher-magnification image of Cre expression neuron (arrow, d–f) from the insets of (c). DAPI counterstaining indicated cell nuclei (blue) (scale bar, 50 μm in a–c and 20 μm in d–f). (B) Left panel: representative western blots of Gab1 and Gab2 from the medial septum of AAV2-Cre-GFP-injected $Gab1^{f/f}$ mice and scrambled-sequence-injected mice. Right panel: quantification of Gab1 protein expression as densitometry ratio of scrambled-sequence-injected mice. $^{***}P < 0.001$ versus scrambled-sequence-injected mice using unpaired two-tailed Student's *t*-test. $n = 6$ mice of each group. Immunoblotting with an anti-β-actin antibody demonstrated equal protein loading in each lane. (C) NORT data from AAV2-Cre-GFP-injected $Gab1^{f/f}$ and scrambled-sequence-injected mice. $Gab1^{f/f}$ mice with or without silence of Gab1 in medial septum were assessed by discrimination index at 2 and 4 weeks after the AAV2-Cre-GFP or scrambled-sequence AAV injection. $^{**}P < 0.01$ and $^{***}P < 0.001$ versus scrambled-sequence-injected mice at indicated time after virus injection using unpaired two-tailed Student's *t*-test. $n = 6$ mice of each group. (D) Y-maze data from AAV2-Cre-GFP-injected $Gab1^{f/f}$ and scrambled-sequence-injected mice. Successful alternation rate was decreased in AAV2-Cre-GFP-injected mice at 2 and 4 weeks after virus injection. $^{***}P < 0.001$ versus scrambled control using unpaired two-tailed Student's *t*-test. $n = 4$–6 mice of each group. Error bars represent mean ± SEM.

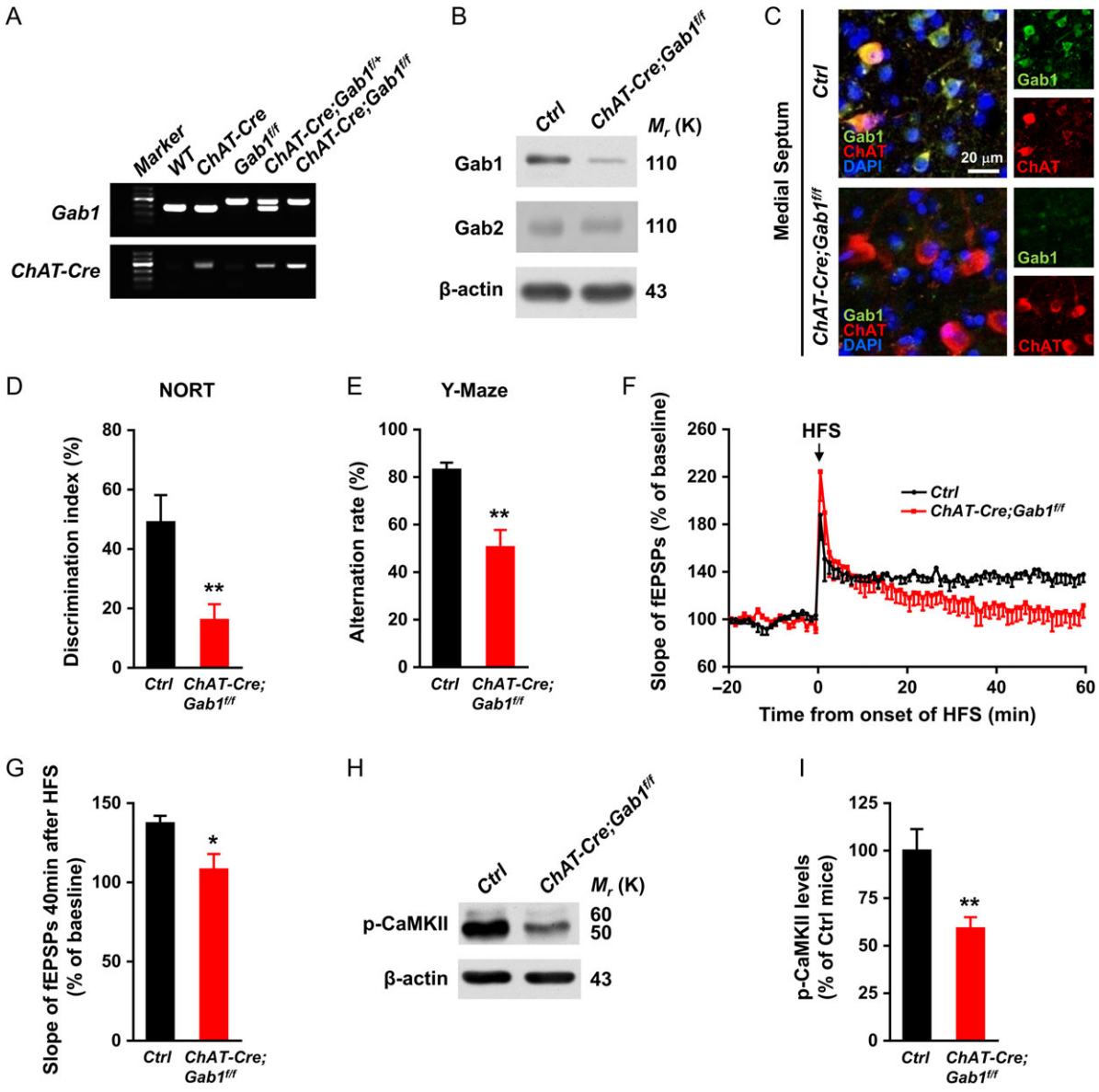

Figure 4. Gab1 knockdown in cholinergic neurons leads to cognitive deficits in adult mice. (*A*) Conditional targeting of the *Gab1* gene. Agarose gel of PCR amplimers for WT, floxed, and knockout *Gab1* alleles from the genomic DNA of mice with different *Gab1* genotypes. (*B*) Gab1 protein levels decreased in the medial septum of *ChAT-Cre;Gab1*$^{f/f}$ mice, but Gab2 did not. Data were the representatives from 3 independent experiments. (*C*) Specific ablation of Gab1 in cholinergic neurons. Immunostaining of the medial septum slices from *Gab1*$^{f/f}$ and *ChAT-Cre;Gab1*$^{f/f}$ mice stained with anti-Gab1 and anti-ChAT antibody, showing the low expression level of Gab1 on ChAT-positive cholinergic neurons. Slices were also stained with DAPI to indicate nuclei (scale bar, 20 μm). (*D*) NORT data from *Gab1*$^{f/f}$ and *ChAT-Cre;Gab1*$^{f/f}$ mice. The differences in exploratory preference of new object were assessed between the groups in the test sessions. $^{**}P < 0.01$ versus *Gab1*$^{f/f}$ mice using unpaired two-tailed Student's *t*-test. $n = 7$ mice of each group. (*E*) Changes in spontaneous alternation behavior in the Y-maze test for *Gab1*$^{f/f}$ and *ChAT-Cre;Gab1*$^{f/f}$ mice. $^{**}P < 0.01$ versus *Gab1*$^{f/f}$ mice using unpaired two-tailed Student's *t*-test. $n = 5$ mice of each group. (*F*) Glutamatergic synaptic plasticity induced by HFS at Schaffer collateral-CA1 synapses in the hippocampus illustrated by field EPSPs recorded in slices from *Gab1*$^{f/f}$ and *ChAT-Cre;Gab1*$^{f/f}$ mice. $n = 5$ slices of *Gab1*$^{f/f}$ and $n = 7$ slices of *ChAT-Cre;Gab1*$^{f/f}$. (*G*) Cumulative data showing mean fEPSP slopes 40 min after HFS from the LTP experiments in (*F*). $^{*}P < 0.05$ versus *Gab1*$^{f/f}$ using unpaired two-tailed Student's *t*-test. (*H*) Representative immunoblot and (*I*) relative density quantification of CaMKII phosphorylation (Thr286) in hippocampus of *Gab1*$^{f/f}$ and *ChAT-Cre;Gab1*$^{f/f}$ mice. $^{**}P < 0.01$ versus *Gab1*$^{f/f}$ using unpaired two-tailed Student's *t*-test. $n = 6$ mice of each group. Immunoblotting with an anti-β-actin antibody demonstrated equal protein loading in each lane. Ctrl, *Gab1*$^{f/f}$. Error bars represent mean ± SEM.

HFS (100 Hz, twice) of the Schaffer collateral/commissural pathways induced long-lasting LTP in the hippocampal CA1 region in *Gab1*$^{f/f}$ mice. In contrast, *ChAT-Cre;Gab1*$^{f/f}$ mice showed markedly reduced LTP (Fig. 4F,G). This effect was associated with a significant decrease in phosphorylation of CaMKII (Thr286) (Fig. 4H,I). Together, the above results suggest that loss of Gab1 in cholinergic neurons leads to cognitive dysfunction.

Increased Excitability of Cholinergic Neurons in Gab1-Deficient Mice

To record from Gab1-expressing cholinergic neurons, brain slices were prepared from *ChAT-eGFP;Gab1*$^{f/f}$ mice (Fig. 5A). Cholinergic neurons in the septum were identified by the presence of GFP and recorded in whole-cell mode (Zaborszky et al. 2008; Ren et al. 2011). In *ChAT-Cre;Gab1*$^{f/f}$ mice, cholinergic

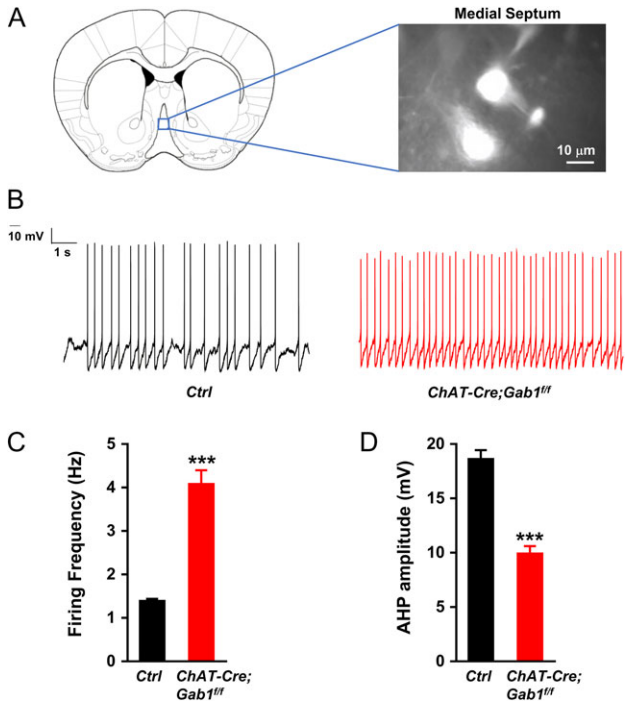

Figure 5. Gab1 deficits significantly increase the excitability of spontaneous cholinergic neurons in the medial septum. (A) CCD images of EGFP-positive neurons recorded in the medial septum area of *ChAT-eGFP* mice (scale bar, 10 μm). (B) Representative spontaneous APs of EGFP-positive neurons recorded in the medial septum of *Gab1$^{f/f}$* and *ChAT-Cre;Gab1$^{f/f}$* mice. (C,D) Firing properties of EGFP-positive neurons in *Gab1$^{f/f}$* and *ChAT-Cre;Gab1$^{f/f}$* mice. The parameters for firing frequency (C), AHP (after-hyperpolarization) amplitude (D) were quantified. $^{***}P < 0.001$ versus *Gab1$^{f/f}$* using unpaired two-tailed Student's *t*-test. $n = 6$ mice of each group. Ctrl, *Gab1$^{f/f}$*. Error bars represent mean ± SEM.

neurons that were spontaneously active showed an increased firing rate compared with those recorded from *ChAT-eGFP;Gab1$^{f/f}$* mice (Fig. 5B,C). This increase in firing was associated with a significant decrease in after-hyperpolarization (AHP) amplitude (Fig. 5D). In addition, in neurons that were not spontaneously active (about 15%), intracellular current injection evoked more spikes in cells lacking Gab1 than those expressing Gab1 (Supplementary Fig. 7). No significant changes in tau, R_{in} and C_m were observed in *ChAT-Cre;Gab1$^{f/f}$* mice (Supplementary Fig. 8).

The decrease in AHP of spontaneous cholinergic neurons suggests a possible change in the small conductance Ca^{2+}-activated K^+ channel (SK channel), which regulates the excitability of neurons and their responsiveness to synaptic input patterns, contributing to the AHP following AP bursts, and curtails EPSPs in neuronal dendrite (Ngo-Anh et al. 2005; Giessel and Sabatini 2010; Maylie and Adelman 2010).

Intriguingly, simulations of the SK channel with agonist (NS309, 5 μM) decreased the firing rate in both *Gab1$^{f/f}$* and *ChAT-Cre;Gab1$^{f/f}$* mice, but its effect was statistically larger in the latter (Fig. 6A,B), which indicated that the functions of SK channel in *ChAT-Cre;Gab1$^{f/f}$* mice were impaired to some extent. In addition, SK channel blockade (apamin, 100 nM) increased AP frequency dramatically in *Gab1$^{f/f}$* mice, mimicking the firing pattern of cholinergic neurons in *ChAT-Cre;Gab1$^{f/f}$* mice, but had no effect in *ChAT-Cre;Gab1$^{f/f}$* mice (Fig. 6A,C), which may suggest that the deficient SK channel function could not be further blocked by apamin. Consistently, similar results were obtained when we matched the firing frequency by analyzing AHP amplitude with SK channel modulator (Fig. 6D,E). The SK channel agonist NS309 (5 μM) increased the AHP in neurons obtained from *ChAT-Cre;Gab1$^{f/f}$* mice (Fig. 6D), whereas apamin (100 nM) significantly reduced the AHP in neurons recorded from *Gab1$^{f/f}$* mice and abolished the AHP difference between the 2 groups of cells (Fig. 6E). The above results suggest that the SK channel is dysfunctional in Gab1 deficit cholinergic neurons and responsible for the decreased AHP amplitude and increased firing in these neurons.

Restoration of Gab1 in Cholinergic Neurons in MS Improves Cognitive Function in *ChAT-Cre;Gab1$^{f/f}$* Mice

To specifically restore Gab1 function in cholinergic neurons, Cre recombinase-dependent Gab1 expression AAV vectors (AAV-Flex-Gab1) were injected into medial septum of *ChAT-Cre;Gab1$^{f/f}$* mice (Fig. 7A), which drive selective Gab1 expression in ChAT-positive cholinergic neurons (Fig. 7B). Three weeks after virus infection, cognitive function-related behavior test was performed. In MWM test, *ChAT-Cre;Gab1$^{f/f}$* mice showed an increase in the escape latency (Fig. 7C) and a decrease in platform crossing number and time spent in the target quadrant in compared with *ChAT-Cre* mice (Fig. 7D,E). By contrast, AAV-Gab1 treatment significantly reversed these effects (Fig. 7C–E). What's more, in both the novel object recognition task and the Y-maze test, selectively re-express Gab1 significantly reversed cognitive deficits in *ChAT-Cre;Gab1$^{f/f}$* mice (Fig. 7F,G).

To further validate the functional importance of Gab1 in cholinergic neurons, we studied the effect of re-express Gab1 on excitability of cholinergic neurons in *ChAT-Cre;Gab1$^{f/f}$* mice after behavior test. The cholinergic neurons upon AAV-Con injection were confirmed by the EGFP expression in *ChAT-Cre* mice and *ChAT-Cre;Gab1$^{f/f}$* mice. Following AAV-Gab1 infection in *ChAT-Cre;Gab1$^{f/f}$* mice, the neurons recorded were confirmed as cholinergic neurons by using lucifer yellow injection combined with post hoc staining for ChAT (Supplementary Fig. 9). Whole-cell patch clamp recordings from these neurons revealed a decreased spontaneous APs in *ChAT-Cre;Gab1$^{f/f}$* mice following AAV-Gab1 injection (Supplementary Fig. 10A,B). Again, we confirmed that conditional restoration of Gab1 rescued the AHP amplitude in cholinergic neurons to a level similar to that observed in *ChAT-Cre* mice (Supplementary Fig. 10C). Specific restoration of Gab1 only in cholinergic neurons is sufficient to maintain MS cholinergic neurons activity.

Expression of Gab1 in the Medial Septum Restores Memory Impaired in *APP^{swe}/PS1* Mice

To explore whether overexpression of Gab1 in medial septum could restore memory impaired in *APP^{swe}/PS1* mice, lentiviral vectors encoding mouse Gab1 (Lenti-Gab1) under CMV promoter or control lentiviral vectors (Lenti-Con) were injected into the medial septum in 6 months old *APP^{swe}/PS1* mice and WT mice. Three weeks after the injection, the Gab1 protein was overexpressed in medial septum of *APP^{swe}/PS1* mice (Supplementary Fig. 11). In the MWM test (Fig. 8A,B), Lenti-Gab1 transduction in the medial septum decreased escape latency in *APP^{swe}/PS1* mice (Fig. 8A) and significantly enhanced platform crossing in the target quadrant (Fig. 8B). The treatment also significantly restored the level of CaMKII (Thr286) and synapsin I (Ser603) phosphorylation in the hippocampus as illustrated by immunoblotting

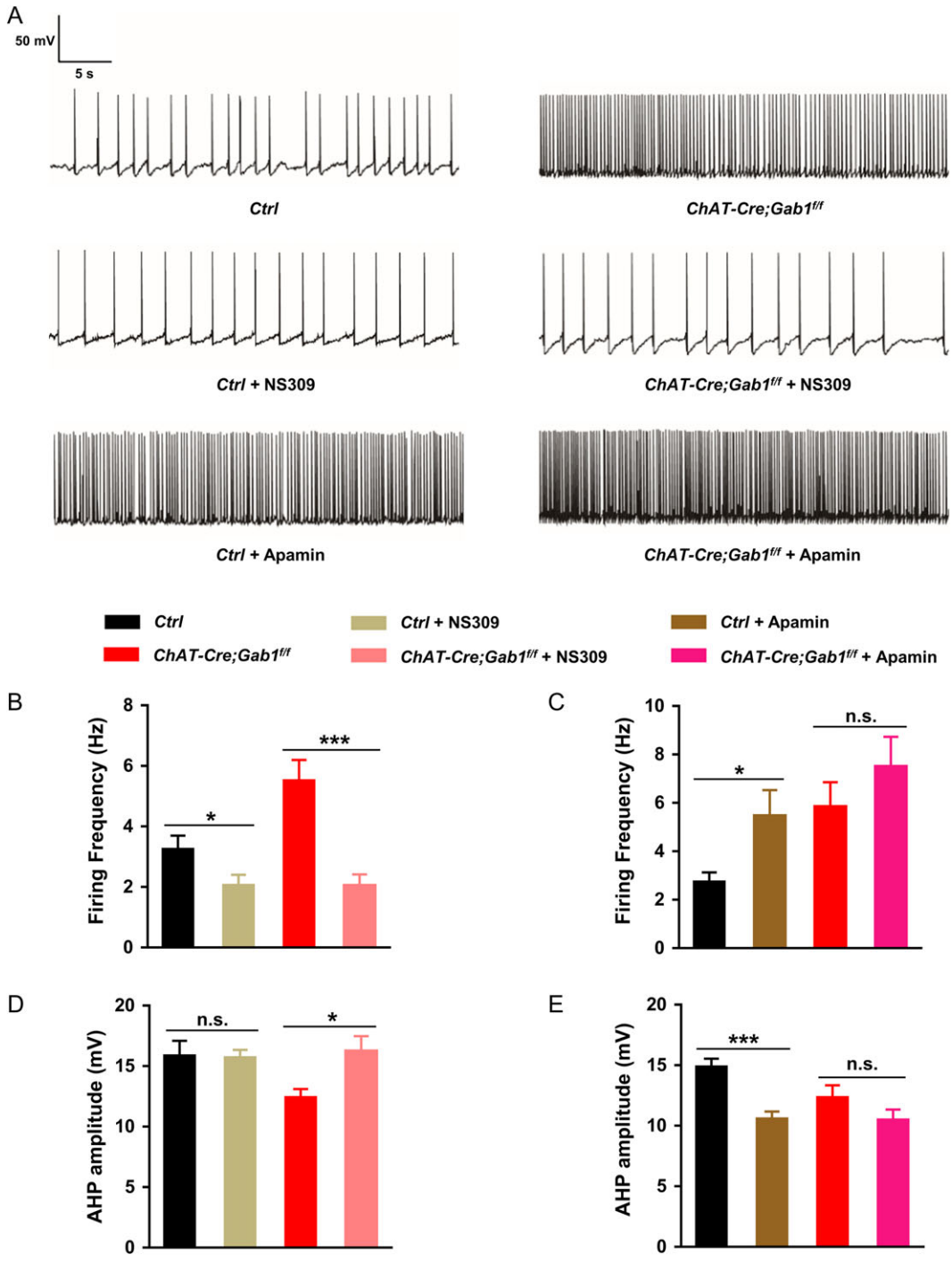

Figure 6. Decreased SK channels mediate the increased excitability of cholinergic neurons in Gab1 deficit mice. (*A*) Representative typical pacemaker-like spontaneous APs of cholinergic neurons recorded in the medial septum of *Gab1*$^{f/f}$ and *ChAT-Cre;Gab1*$^{f/f}$ mice in the presence of the SK channel modulator NS309 (5 μM) or apamin (100 nM). (*B*) Stimulations of the SK channel with agonist (NS309, 5 μM) decreased AP frequency in control and *ChAT-Cre;Gab1*$^{f/f}$ mice. $^{*}P < 0.05$ versus no treatment in *Gab1*$^{f/f}$ mice; $^{***}P < 0.001$ versus no treatment in *ChAT-Cre;Gab1*$^{f/f}$ mice using unpaired two-tailed Student's *t*-test. $n = 5$ mice of each group. (*C*) Effect of apamin (100 nM) on AP frequency in control and *ChAT-Cre;Gab1*$^{f/f}$ mice. $^{*}P < 0.05$ versus no treatment in *Gab1*$^{f/f}$ mice using unpaired two-tailed Student's *t*-test. $n = 4$–5 mice of each group. (*D*) Summary graph of AHP amplitude measured following NS309 (5 μM) treatment. $^{*}P < 0.05$ versus no treatment in *ChAT-Cre;Gab1*$^{f/f}$ mice using unpaired two-tailed Student's *t*-test. $n = 5$ mice of each group. (*E*) Summary graph of AHP amplitude measured following apamin (100 nM) treatment in control and *ChAT-Cre;Gab1*$^{f/f}$ mice. $^{***}P < 0.001$ versus no treatment in *Gab1*$^{f/f}$ mice using unpaired two-tailed Student's *t*-test. $n = 4$–5 mice of each group. n.s., no significant. Ctrl, *Gab1*$^{f/f}$. Error bars represent mean ± S.E.M.

(Fig. 8C,D) and immunohistochemistry (Fig. 8E,F). Thus, upregulation the expression level of Gab1 in the medial septum was enough to significantly improve cognitive function in AD mice.

Discussion

Here, we provide, for the first time, the evidence that Gab1 is selectively expressed in central cholinergic neurons and

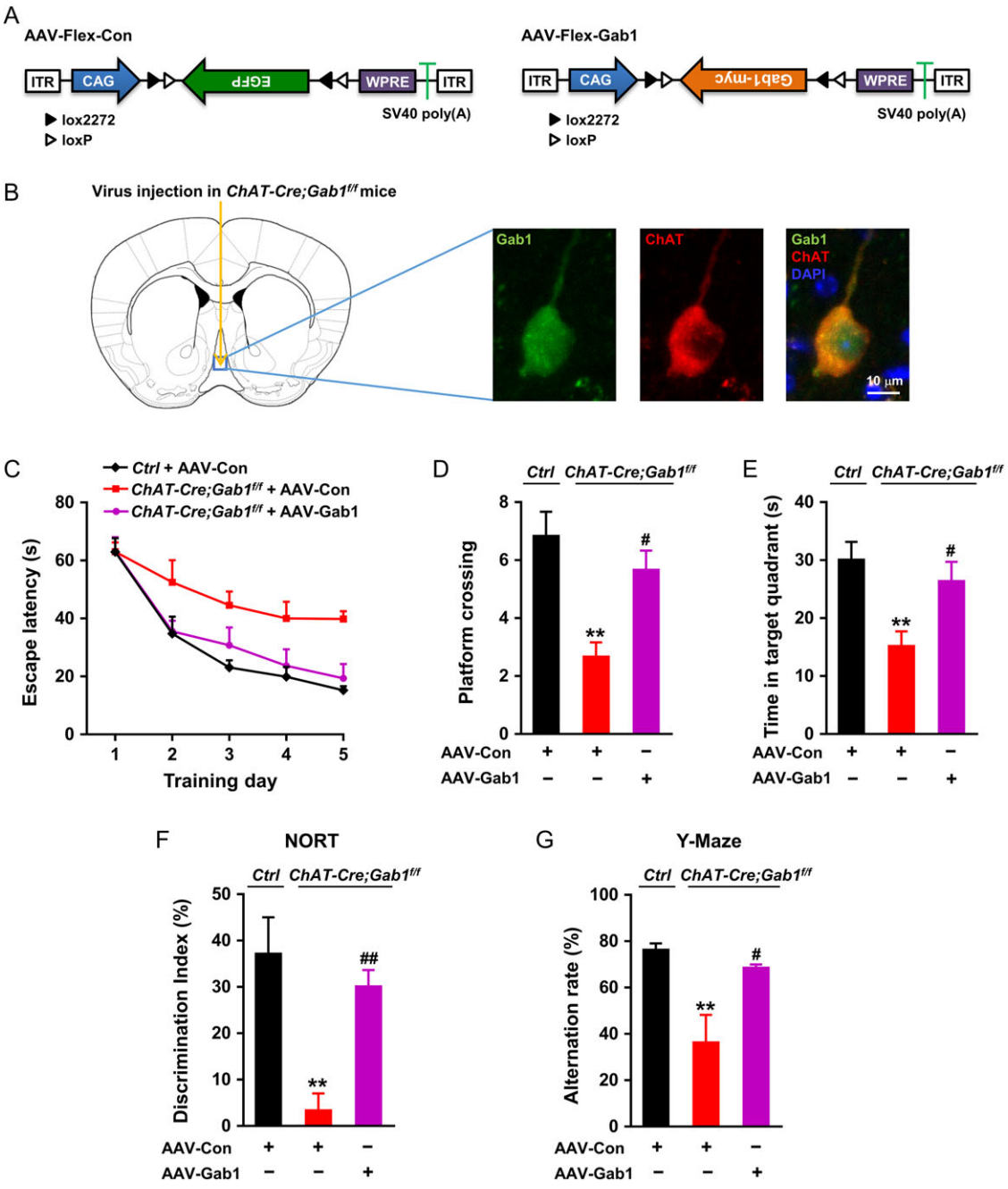

Figure 7. Selectively re-expression of Gab1 in MS cholinergic neurons rescues cognitive dysfunction in Gab1 conditional knockout mice. (*A*) Strategies for cholinergic neuron-specific Gab1 expression with a flip-excision (Flex) switch in the presence of Cre recombinase. AAV-Flex-Con (or AAV-Con) and AAV-Flex-Gab1 (or AAV-Gab1) viral constructs were prepared. (*B*) Left: Illustration of viral injection in MS. Right: Fluorescence images showing re-expression of Gab1 (Green) in MS cholinergic neurons (ChAT positive, Red) of *ChAT-Cre;Gab1*$^{f/f}$ mice 3 weeks after AAV-Flex-Gab1 injection. DAPI counterstaining indicated nuclei (blue) (scale bar, 10 μm). (*C*) Escape latency (time to find the hidden platform) in the MWM test plotted against the training days. Acquisition of the reference memory task as expressed by the escape latency (in seconds) over 5-day training (4 trials every day). Two-way ANOVA followed by Tukey's post hoc multiple comparison tests. *ChAT-Cre;Gab1*$^{f/f}$ + AAV-Con versus *Ctrl* mice + AAV-Con: $P < 0.001$; *ChAT-Cre;Gab1*$^{f/f}$ + AAV-Gab1 versus *ChAT-Cre;Gab1*$^{f/f}$ + AAV-Con: $P < 0.001$. $n = 6$ mice of each group. (*D*–*E*) AAV-Gab1 transduction improved the spatial memory of *ChAT-Cre;Gab1*$^{f/f}$ mice as showed in platform crossing (*D*) and time in target quadrant (in seconds) (*E*) during a 60 s probe trial of MWM test. $^{**}P < 0.01$ versus *Ctrl* mice with AAV-Con injection; $^{\#}P < 0.05$ versus *ChAT-Cre;Gab1*$^{f/f}$ mice with AAV-Con injection using one-way ANOVA followed by Tukey's post hoc test. $n = 6$ mice of each group. (*F*) AAV-Gab1 brain transduction improved the discrimination index of *ChAT-Cre;Gab1*$^{f/f}$ mice, as assessed by the NORT. $^{**}P < 0.01$ versus *Ctrl* mice with AAV-Con injection; $^{\#\#}P < 0.01$ versus *ChAT-Cre;Gab1*$^{f/f}$ mice with AAV-Con injection using one-way ANOVA followed by Tukey's post hoc test. $n = 6$ mice of each group. (*G*) AAV-Gab1 transduction increased successful alternations of *ChAT-Cre;Gab1*$^{f/f}$ mice in the Y-maze test. $^{**}P < 0.01$ versus *Ctrl* mice with AAV-Con injection; $^{\#}P < 0.05$ versus *ChAT-Cre;Gab1*$^{f/f}$ mice with AAV-Con injection using one-way ANOVA followed by Tukey's post hoc test. $n = 6$ mice of each group. *Ctrl*, *ChAT-Cre* mice. Error bars represent mean ± SEM.

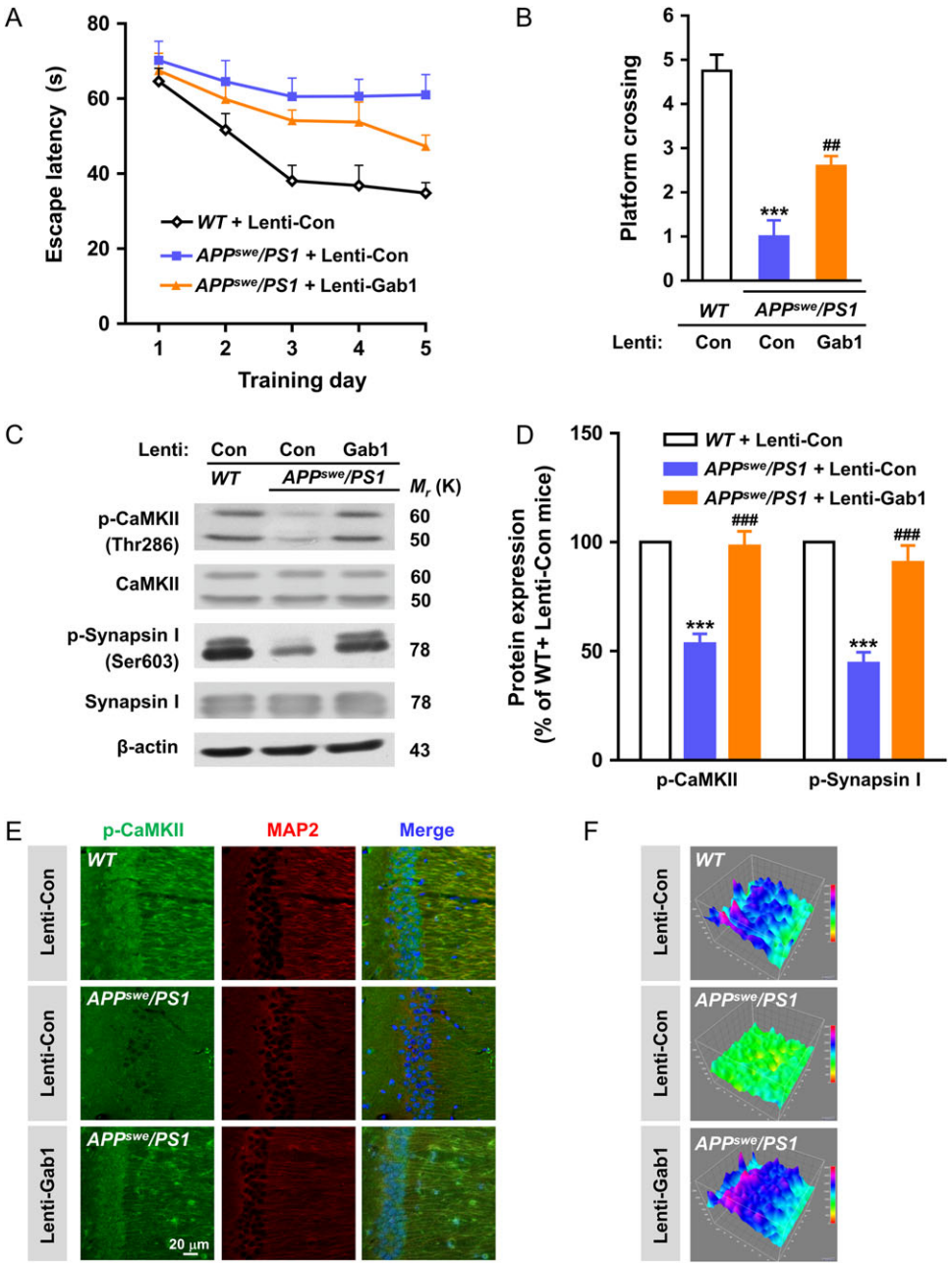

Figure 8. Spatial memory deficits in APP^{swe}/PS1 AD model mice are alleviated by Lentiviral-Gab1 brain transduction. (*A*) Escape latency (time to find the hidden platform) in the MWM test plotted against the training days. Acquisition of the reference memory task as expressed by the escape latency (in seconds) over 5-day training (4 trials every day). Two-way ANOVA followed by Tukey's post hoc multiple comparison tests. APP^{swe}/PS1 mice with lenti-Con versus WT mice with lenti-Con: $P < 0.001$. APP^{swe}/PS1 mice with lenti-Gab1 versus APP^{swe}/PS1 mice with lenti-Con: $P < 0.05$. WT + Lenti-Con ($n = 9$), APP^{swe}/PS1 + Lenti-Con ($n = 14$), APP^{swe}/PS1 + Lenti-Gab1 ($n = 13$). (*B*) Lentiviral-Gab1 transduction increased the platform crossing in the target quadrant in APP^{swe}/PS1 mice during a 60 s probe trial in the MWM test. $^{***}P < 0.001$ versus WT mice with lenti-Con; $^{\#\#}P < 0.01$ versus APP^{swe}/PS1 mice with lenti-Con treatment using one-way ANOVA followed by Tukey's post hoc test. WT + Lenti-Con ($n = 8$), APP^{swe}/PS1 + Lenti-Con ($n = 10$), APP^{swe}/PS1 + Lenti-Gab1 ($n = 10$). (*C*) Immunoblots demonstrated changes in CaMKII (Thr286) phosphorylation and synapsin I (Ser603) phosphorylation 3 weeks after lentiviral-Gab1 or lentiviral-Con treatment in APP^{swe}/PS1 mice. Representative images of immunoblots using antibodies against autophosphorylated CaMKII (Thr286), CaMKII, phosphorylated synapsin I (Ser603), and synapsin I. Immunoblotting with an anti-β-actin antibody demonstrated equal protein loading in each lane. (*D*) Quantitative analyses of autophosphorylated CaMKII (Thr286) and phosphorylated synapsin I (Ser603) as analyzed by densitometry. Data are expressed as the percentage of value of WT mice with lenti-Con. $^{***}P < 0.001$ versus WT mice with lenti-Con; $^{\#\#\#}P < 0.001$ versus APP^{swe}/PS1 mice with lenti-Con using one-way ANOVA followed by Tukey's post hoc test. $n = 5$ mice of each group. Error bars represent mean ± SEM. (*E*) Immunohistochemical data for the effect of lentivirus Gab1 expression on hippocampal CA1 CaMKII autophosphorylation in APP^{swe}/PS1 mice. The expression of phospho-CaMKII (Thr286) (green) and MAP2 (red) was examined in the hippocampus of CA1 region at indicated groups. DAPI counterstaining (blue) indicated nuclear localization (Scale bar, 20 μm). Data were the representatives from 3 independent experiments. (*F*) Visualization of color scale intensities of phospho-CaMKII in stratum pyramidale of CA1 through 3D surface plots.

downregulated in AD patient and mice. In mice, selective downregulation of Gab1 in the septum impaired learning and memory, whereas overexpression of Gab1 in the same area rescued the cognitive deficits seen in *ChAT-Cre;Gab1$^{f/f}$ and APP^{swe}/PS1* mice.

The medial septum region sends cholinergic, GABAergic, and glutamatergic projections to the hippocampus (Lewis and Shute 1967; Kohler et al. 1984; Sotty et al. 2003; Colom et al. 2005; Henny and Jones 2008). In the present study, we showed that Gab1 was selectively located in cholinergic neurons, and not observed in GAD65-, PV-, or CaMKIIα-immunoreactive cells. The finding that downregulation of Gab1 in septal cholinergic neurons caused cognitive deficits further suggested that Gab1 plays a critical role in cholinergic projection neurons.

Dysfunction of cholinergic neurons in the basal forebrain correlates with the cognitive impairment in AD patients (Bonsi et al. 2004; Berson et al. 2012). Our results suggest that Gab1 in cholinergic neurons may play a role in the cognitive dysfunction. We found that mice lacking Gab1 in cholinergic neurons, that is, *ChAT-Cre;Gab1$^{f/f}$* mice, exhibited significant cognitive deficits as measured by the MWM, new object recognition and Y-maze tests. These tasks are known to be sensitive to the integrity of septo-hippocampal projections. This finding is consistent with the fact that Gab1 is selectively expressed in cholinergic neurons and *CaMKIIα-Cre;Gab1$^{f/f}$* mice showed no significant changes in either the number or size of Gab1-positive neurons in brain. In line with a role of the medial septum in hippocampus-dependent learning and memory (Sava and Markus 2008; Sanchez-Ortiz et al. 2012), knockdown of Gab1 decreased the phosphorylation of CaMKII (Thr286) in the hippocampus and impaired hippocampal LTP.

Changes discussed above suggest that Gab1 deletion may lead to an inhibition of septal cholinergic neurons projecting to the hippocampus. To our surprise, both the spontaneous and evoked firing activities were increased in septal cholinergic neurons in *ChAT-Cre;Gab1$^{f/f}$* mice. The hyperexcitability of spontaneous cholinergic neurons was associated with a decrease in the amplitude of AHP. Further experiments suggest that the SK channel, which modulates firing frequency and partially contributes to the AHP that follows the bursts of APs (Sah 1996; Stocker et al. 1999; Edgerton and Reinhart 2003), is present but dysfunctional in Gab1-deficient cells. Thus, in these cells, the SK channel enhancer NS309 could still significantly increase the AHP and decrease firing frequency. This effect was completely abolished by the selective SK channel blocker apamin. We speculate that this increase in firing activity is a compensatory change of cholinergic neurons due to reduced release of acetylcholine from their axon terminals.

The importance of Gab1 in cholinergic neurons is further highlighted by the finding that its expression is significantly decreased in both AD patient and an animal model of AD, that is, *APP^{swe}/PS1* mice. Here, our ^{18}F-FDG microPET imaging data indicated that Gab1 treatment had no effect on metabolic activity of glucose in *APP^{swe}/PS1* mice (Supplementary Fig. 12). More importantly, we found that enhancement of Gab1 expression by genetic manipulation restored the memory impaired in *ChAT-Cre;Gab1$^{f/f}$* and *APP^{swe}/PS1* mice, indicating that Gab1 signaling may serve as a potential treatment target for disorders involving dysfunction of central cholinergic neurons including AD.

Supplementary Material

Supplementary material is available at *Cerebral Cortex* online.

Authors' Contributions

N.L., C.T., Y.L., and F.H. participated in the designing, performing experiments, and data analysis. N.S., L.S., X.L., Y.G., R.T., Q.J., C.W., J.H., K.Z., G.W., and Z.L. assisted with the experiments and data analysis. K.F. revised the manuscript and provided supervisory support. Y.L. and F.H. discussed, designed the experiments, and co-wrote the manuscript.

Funding

This work was supported in part by The National Key Research and Development Program of China (2016YFE0125400); National Natural Science Foundations of China (81120108023, 91232705, 81473202) and Science Technology of Zhejiang Province (2015C33250); The Zhejiang Province Program for Cultivation of High-level Health talents; New Century 151 Talent Project of Zhejiang Province.

Notes

We thank the Imaging Center, Core Facilities of Zhejiang University School of Medicine for their valuable contributions. We also thank the Duke Center for In Vivo Microscopy (supported by NIH/NIBIB P41 EB015897) of using their mice atlas data for our microPET analysis. *Conflicts of Interest*: None declared.

References

Bard-Chapeau EA, Hevener AL, Long S, Zhang EE, Olefsky JM, Feng GS. 2005. Deletion of Gab1 in the liver leads to enhanced glucose tolerance and improved hepatic insulin action. Nat Med. 11:567–571.

Bennett BD, Callaway JC, Wilson CJ. 2000. Intrinsic membrane properties underlying spontaneous tonic firing in neostriatal cholinergic interneurons. J Neurosci. 20:8493–8503.

Berson A, Barbash S, Shaltiel G, Goll Y, Hanin G, Greenberg DS, Ketzef M, Becker AJ, Friedman A, Soreq H. 2012. Cholinergic-associated loss of hnRNP-A/B in Alzheimer's disease impairs cortical splicing and cognitive function in mice. EMBO Mol Med. 4:730–742.

Bonsi P, De Persis C, Calabresi P, Bernardi G, Pisani A. 2004. Coordinate high-frequency pattern of stimulation and calcium levels control the induction of LTP in striatal cholinergic interneurons. Learn Mem. 11:755–760.

Cao C, Rioult-Pedotti MS, Migani P, Yu CJ, Tiwari R, Parang K, Spaller MR, Goebel DJ, Marshall J. 2013. Impairment of TrkB-PSD-95 signaling in Angelman syndrome. PLoS Biol. 11: e1001478.

Christensen H, Maltby N, Jorm AF, Creasey H, Broe GA. 1992. Cholinergic 'blockade' as a model of the cognitive deficits in Alzheimer's disease. Brain. 115(Pt 6):1681–1699.

Colom LV, Castaneda MT, Reyna T, Hernandez S, Garrido-Sanabria E. 2005. Characterization of medial septal glutamatergic neurons and their projection to the hippocampus. Synapse. 58:151–164.

Dixit M, Loot AE, Mohamed A, Fisslthaler B, Boulanger CM, Ceacareanu B, Hassid A, Busse R, Fleming I. 2005. Gab1, SHP2, and protein kinase A are crucial for the activation of the endothelial NO synthase by fluid shear stress. Circ Res. 97:1236–1244.

Edgerton JR, Reinhart PH. 2003. Distinct contributions of small and large conductance Ca2+-activated K+ channels to rat Purkinje neuron function. J Physiol. 548:53–69.

Eulenfeld R, Schaper F. 2009. A new mechanism for the regulation of Gab1 recruitment to the plasma membrane. J Cell Sci. 122:55–64.

Fukunaga K, Goto S, Miyamoto E. 1988. Immunohistochemical localization of Ca2+/calmodulin-dependent protein kinase II in rat brain and various tissues. J Neurochem. 51:1070–1078.

Fukunaga K, Soderling TR, Miyamoto E. 1992. Activation of Ca2+/-calmodulin-dependent protein kinase II and protein kinase C by glutamate in cultured rat hippocampal neurons. J Biol Chem. 267:22527–22533.

Giessel AJ, Sabatini BL. 2010. M1 muscarinic receptors boost synaptic potentials and calcium influx in dendritic spines by inhibiting postsynaptic SK channels. Neuron. 68:936–947.

Goekoop R, Scheltens P, Barkhof F, Rombouts SA. 2006. Cholinergic challenge in Alzheimer patients and mild cognitive impairment differentially affects hippocampal activation–a pharmacological fMRI study. Brain. 129:141–157.

Gong N, Li Y, Cai GQ, Niu RF, Fang Q, Wu K, Chen Z, Lin LN, Xu L, Fei J, et al. 2009. GABA transporter-1 activity modulates hippocampal theta oscillation and theta burst stimulation-induced long-term potentiation. J Neurosci. 29:15836–15845.

Gu Z, Yakel JL. 2011. Timing-dependent septal cholinergic induction of dynamic hippocampal synaptic plasticity. Neuron. 71:155–165.

Han F, Shioda N, Moriguchi S, Qin ZH, Fukunaga K. 2008. The vanadium (IV) compound rescues septo-hippocampal cholinergic neurons from neurodegeneration in olfactory bulbectomized mice. Neuroscience. 151:671–679.

Han F, Shioda N, Moriguchi S, Yamamoto Y, Raie AY, Yamaguchi Y, Hino M, Fukunaga K. 2008. Spiro[imidazo[1,2-a]pyridine-3,2-indan]-2(3H)-one (ZSET1446/ST101) treatment rescues olfactory bulbectomy-induced memory impairment by activating Ca2+/calmodulin kinase II and protein kinase C in mouse hippocampus. J Pharmacol Exp Ther. 326: 127–134.

Hangya B, Borhegyi Z, Szilagyi N, Freund TF, Varga V. 2009. GABAergic neurons of the medial septum lead the hippocampal network during theta activity. J Neurosci. 29: 8094–8102.

Henny P, Jones BE. 2008. Projections from basal forebrain to prefrontal cortex comprise cholinergic, GABAergic and glutamatergic inputs to pyramidal cells or interneurons. Eur J Neurosci. 27:654–670.

Ishiguro K, Sato K, Takamatsu M, Park J, Uchida T, Imahori K. 1995. Analysis of phosphorylation of tau with antibodies specific for phosphorylation sites. Neurosci Lett. 202:81–84.

Ji D, Lape R, Dani JA. 2001. Timing and location of nicotinic activity enhances or depresses hippocampal synaptic plasticity. Neuron. 31:131–141.

Johnson GA, Badea A, Brandenburg J, Cofer G, Fubara B, Liu S, Nissanov J. 2010. Waxholm space: an image-based reference for coordinating mouse brain research. Neuroimage. 53: 365–372.

Kaifosh P, Lovett-Barron M, Turi GF, Reardon TR, Losonczy A. 2013. Septo-hippocampal GABAergic signaling across multiple modalities in awake mice. Nat Neurosci. 16:1182–1184.

Kohler C, Chan-Palay V, Wu JY. 1984. Septal neurons containing glutamic acid decarboxylase immunoreactivity project to the hippocampal region in the rat brain. Anat Embryol (Berl). 169:41–44.

Korhonen JM, Said FA, Wong AJ, Kaplan DR. 1999. Gab1 mediates neurite outgrowth, DNA synthesis, and survival in PC12 cells. J Biol Chem. 274:37307–37314.

Lewis PR, Shute CC. 1967. The cholinergic limbic system: projections to hippocampal formation, medial cortex, nuclei of the ascending cholinergic reticular system, and the subfornical organ and supra-optic crest. Brain. 90:521–540.

Li KX, Lu YM, Xu ZH, Zhang J, Zhu JM, Zhang JM, Cao SX, Chen XJ, Chen Z, Luo JH, et al. 2011. Neuregulin 1 regulates excitability of fast-spiking neurons through Kv1.1 and acts in epilepsy. Nat Neurosci. 15:267–273.

Liu J, Fukunaga K, Yamamoto H, Nishi K, Miyamoto E. 1999. Differential roles of Ca(2+)/calmodulin-dependent protein kinase II and mitogen-activated protein kinase activation in hippocampal long-term potentiation. J Neurosci. 19: 8292–8299.

Lu Y, Xiong Y, Huo Y, Han J, Yang X, Zhang R, Zhu DS, Klein-Hessling S, Li J, Zhang X, et al. 2011. Grb-2-associated binder 1 (Gab1) regulates postnatal ischemic and VEGF-induced angiogenesis through the protein kinase A-endothelial NOS pathway. Proc Natl Acad Sci USA. 108:2957–2962.

Lu YM, Huang JY, Wang H, Lou XF, Liao MH, Hong LJ, Tao RR, Ahmed MM, Shan CL, Wang XL, et al. 2014. Targeted therapy of brain ischaemia using Fas ligand antibody conjugated PEG-lipid nanoparticles. Biomaterials. 35:530–537.

Mahmood Q, Wang GF, Wu G, Wang H, Zhou CX, Yang HY, Liu ZR, Han F, Zhao K. 2017. Salvianolic acid A inhibits calpain activation and eNOS uncoupling during focal cerebral ischemia in mice. Phytomedicine. 25:8–14.

Maylie J, Adelman JP. 2010. Cholinergic signaling through synaptic SK channels: it's a protein kinase but which one? Neuron. 68:809–811.

Mitsushima D, Sano A, Takahashi T. 2013. A cholinergic trigger drives learning-induced plasticity at hippocampal synapses. Nat Commun. 4:2760.

Mood K, Saucier C, Bong YS, Lee HS, Park M, Daar IO. 2006. Gab1 is required for cell cycle transition, cell proliferation, and transformation induced by an oncogenic met receptor. Mol Biol Cell. 17:3717–3728.

Morris R. 1984. Developments of a water-maze procedure for studying spatial learning in the rat. J Neurosci Methods. 11: 47–60.

Ngo-Anh TJ, Bloodgood BL, Lin M, Sabatini BL, Maylie J, Adelman JP. 2005. SK channels and NMDA receptors form a Ca2+-mediated feedback loop in dendritic spines. Nat Neurosci. 8:642–649.

Okada H, Ouchi Y, Ogawa M, Futatsubashi M, Saito Y, Yoshikawa E, Terada T, Oboshi Y, Tsukada H, Ueki T, et al. 2013. Alterations in alpha4beta2 nicotinic receptors in cognitive decline in Alzheimer's aetiopathology. Brain. 136: 3004–3017.

Pa J, Berry AS, Compagnone M, Boccanfuso J, Greenhouse I, Rubens MT, Johnson JK, Gazzaley A. 2013. Cholinergic enhancement of functional networks in older adults with mild cognitive impairment. Ann Neurol. 73:762–773.

Ren J, Qin C, Hu F, Tan J, Qiu L, Zhao S, Feng G, Luo M. 2011. Habenula "cholinergic" neurons co-release glutamate and acetylcholine and activate postsynaptic neurons via distinct transmission modes. Neuron. 69:445–452.

Sah P. 1996. Ca(2+)-activated K+ currents in neurones: types, physiological roles and modulation. Trends Neurosci. 19: 150–154.

Sanchez-Ortiz E, Yui D, Song D, Li Y, Rubenstein JL, Reichardt LF, Parada LF. 2012. TrkA gene ablation in basal forebrain results in dysfunction of the cholinergic circuitry. J Neurosci. 32:4065–4079.

Sava S, Markus EJ. 2008. Activation of the medial septum reverses age-related hippocampal encoding deficits: a place field analysis. J Neurosci. 28:1841–1853.

Schaeper U, Vogel R, Chmielowiec J, Huelsken J, Rosario M, Birchmeier W. 2007. Distinct requirements for Gab1 in Met and EGF receptor signaling in vivo. Proc Natl Acad Sci USA. 104:15376–15381.

Sotty F, Danik M, Manseau F, Laplante F, Quirion R, Williams S. 2003. Distinct electrophysiological properties of glutamatergic, cholinergic and GABAergic rat septohippocampal neurons: novel implications for hippocampal rhythmicity. J Physiol. 551:927–943.

Stocker M, Krause M, Pedarzani P. 1999. An apamin-sensitive Ca2+-activated K+ current in hippocampal pyramidal neurons. Proc Natl Acad Sci USA. 96:4662–4667.

Tao RR, Wang H, Hong LJ, Huang JY, Lu YM, Liao MH, Ye WF, Lu NN, Zhu DY, Huang Q, et al. 2014. Nitrosative stress induces peroxiredoxin 1 ubiquitination during ischemic insult via E6AP activation in endothelial cells both in vitro and in vivo. Antioxid Redox Signal. 21:1–16.

Wang H, Hong LJ, Huang JY, Jiang Q, Tao RR, Tan C, Lu NN, Wang CK, Ahmed MM, Lu YM, et al. 2015. P2RX7 sensitizes Mac-1/ICAM-1-dependent leukocyte-endothelial adhesion and promotes neurovascular injury during septic encephalopathy. Cell Res. 25:674–690.

Yang Y, Paspalas CD, Jin LE, Picciotto MR, Arnsten AF, Wang M. 2013. Nicotinic alpha7 receptors enhance NMDA cognitive circuits in dorsolateral prefrontal cortex. Proc Natl Acad Sci USA. 110:12078–12083.

Yang Z, Xue B, Umitsu M, Ikura M, Muthuswamy SK, Neel BG. 2012. The signaling adaptor GAB1 regulates cell polarity by acting as a PAR protein scaffold. Mol Cell. 47:469–483.

Zaborszky L, Hoemke L, Mohlberg H, Schleicher A, Amunts K, Zilles K. 2008. Stereotaxic probabilistic maps of the magnocellular cell groups in human basal forebrain. Neuroimage. 42:1127–1141.

Zhang Y, Xu Y, Liu S, Guo X, Cen D, Xu J, Li H, Li K, Zeng C, Lu L, et al. 2016. Scaffolding protein Gab1 regulates myeloid dendritic cell migration in allergic asthma. Cell Res. 26: 1226–1241.